

1 Three-way Calibration Checks Using Ground-Based, Ship-Based 2 and Spaceborne Radars

3 Alain Protat ¹, Valentin Louf ¹, Joshua Soderholm ¹, Jordan Brook ², William Ponsonby ³

4 ¹ Australian Bureau of Meteorology, Melbourne, Australia

5 ² University of Queensland, Brisbane, Australia

6 ³ Engineering and Technology Program, CSIRO National Collections and Marine Infrastructure, Hobart, Australia

7 *Correspondence to:* Alain Protat (alain.protat@bom.gov.au)

8 **Abstract.**

9 This study uses ship-based weather radar observations collected from *Research Vessel Investigator* to evaluate the
10 Australian weather radar network calibration monitoring technique that uses spaceborne radar observations from the
11 NASA Global Precipitation Mission (GPM). Quantitative operational applications such as rainfall and hail
12 nowcasting require a calibration accuracy of ± 1 dB for radars of the Australian network covering capital cities.
13 Seven ground-based radars along the western coast of Australia and the ship-based OceanPOL radar are first
14 calibrated independently using GPM radar overpasses over a 3-month period. The calibration difference between the
15 OceanPOL radar (used as a moving reference for the second step of the study) and each of the 7 operational radars is
16 then estimated using collocated, gridded, radar observations to quantify the accuracy of the GPM technique. For all
17 seven radars the calibration difference with the ship radar lies within ± 0.5 dB, therefore fulfilling the 1 dB
18 requirement. This result validates the concept of using the GPM spaceborne radar observations to calibrate national
19 weather radar networks (provided that the spaceborne radar maintains a high calibration accuracy). The analysis of
20 the day-to-day and hourly variability of calibration differences between the OceanPOL and Darwin (Berrimah)
21 radars also demonstrates that quantitative comparisons of gridded radar observations can accurately track daily and
22 hourly calibration differences between pairs of operational radars with overlapping coverage (daily and hourly
23 standard deviations of ~ 0.3 dB and ~ 1 dB, respectively).

24 **1 Introduction**

25 Operational radar networks play a major role in providing situational awareness and nowcasting in severe
26 weather situations, including heavy rain, flash floods, hailstorms, and wind gusts. Such radar-based information is
27 then used by forecasters as guidance for issuing severe weather warnings. The quality of these radar-derived
28 products in real-time is driven to a large extent by how well the underlying radar measurements are calibrated.
29 Recently, the Australian Bureau of Meteorology (BoM) has developed an operational radar calibration framework to
30 monitor the calibration of all BoM operational radars in real-time (Louf et al. 2019, hereafter L19). This approach is
31 based on a combination of three techniques. The objective of this technique is to achieve an absolute calibration
32 accuracy better than 1 dB, which is the operational calibration requirement in Australia for quantitative use of the
33 Australian weather radar observations over capital cities (so-called Tier 1 radars). At the heart of this framework lies
34 the so-called Volume Matching Method (VMM), initially developed by Schwaller and Morris (2011) and further

35 improved by Warren et al. (2018, hereafter W18). In this VMM technique, intersections between individual ground-
36 based radar beams and NASA Tropical Rainfall Measurement Mission (TRMM, Simpson et al. 1996) or Global
37 Precipitation Mission (GPM, Hou et al. 2014) scanning Ku-band radar beams are averaged over an optimally
38 defined common sampling volume (see W18 for more detail). In what follows, we will use the term "calibration" to
39 refer to calibration differences between ground or ship-based radars and the GPM radar taken as the "reference".
40 However, it must be noted that reflectivities measured by the GPM radar are not a normed reference, which implies
41 that our use of the term "calibration" is strictly not correct.

42 A major advantage of using the GPM VMM technique is that the spaceborne radar provides a single source
43 of reference to calibrate all radars of an operational network. [This was also well demonstrated in Kollias et al.
44 \(2019\) in the context of calibrating the U.S. Atmospheric Radiation Measurement \(ARM\) cloud radar network using
45 the spaceborne CloudSat radar.](#) Despite multiple possible sources of errors contributing to the VMM calibration
46 error estimate, such as temporal mismatch, imperfect attenuation corrections, gridding and range effects, and
47 differences in radar minimum detectable signal, the overall accuracy of such technique is thought to be better than 2
48 dB for individual overpasses (Schwaller and Morris, 2011; W18; L19). It must be noted however that there has been
49 no independent quantification of this accuracy. This is the main objective of this study, where we use dual-
50 polarization C-band weather radar (OceanPOL) observations collected on board the Marine National Facility (MNF)
51 Research Vessel (RV) Investigator between Darwin and Perth, Australia, as part of the *Years of the Maritime
52 Continent – Australia* (YMCA, Protat et al. 2020) and the *Optimizing Radar Calibration and Attenuation
53 corrections* (ORCA) experiments to evaluate the approach of calibrating a whole radar network using GPM. The
54 concept of this study is presented in Fig. 1. GPM observations are first used to calibrate both the ship-based radar
55 and all the operational ground-based radars along the western coast of Australia independently. The ship-based radar
56 observations calibrated using GPM are then individually compared with those from each ground-based radar as the
57 ship sails close to them. Since all radars (including OceanPOL) have been calibrated using GPM, the differences
58 between ship-based and ground-based observations can be interpreted as an error estimate of the GPM calibration
59 technique, with some unknown additional contribution from errors due to the ship-ground radar comparisons
60 themselves. These errors coming from ship-ground comparisons are expected to be much lower than those arising
61 from the GPM / ground radar comparisons. Indeed, the advantage of using a ship-based radar relative to a
62 spaceborne radar is that many of the error sources in ground-based / satellite radar comparisons are reduced to a
63 minimum. Taking advantage of a month-long dataset of calibration difference estimates between OceanPOL and the
64 Darwin radar, we also assess the operational potential of daily and calibration change monitoring using overlapping
65 ground-based radar observations.

66 The remainder of this paper is organized as follows. In section 2, we briefly describe the YMCA and
67 ORCA experiments, the characteristics of radars used in this study, and the calibration techniques. In section 3, we
68 present the main findings of this study. Concluding remarks are presented in section 4.

69 **2 Radar observations during YMCA and ORCA and calibration comparisons**

70 In this section, we briefly introduce the datasets collected during the YMCA and ORCA experiments, the
71 details of all radars involved in this study, and the techniques used to calibrate the ground and ship radars with the
72 spaceborne radar and to compare ground and ship radars.

Deleted: ¶

74 **2.1 The YMCA and ORCA experiments**

75 *RV Investigator* OceanPOL radar observations used in this study were collected as part of two back-to-back
76 field experiments. The first experiment is the Australian contribution to the Years of the Maritime Continent
77 (YMCA), which is an international coordinated effort to better understand the organization of coastally induced
78 convection over the Maritime Continent and its complex interactions with large-scale drivers, with the ambition to
79 better represent these processes in global circulation models characterized by large and persistent rainfall biases.
80 During the second phase of YMCA (12 November– 19 December 2019), the sampling strategy was to position *RV*
81 *Investigator* off the coast around Darwin in a dual-Doppler configuration with either the Warruwi (north-east of
82 Darwin) or Berrimah (Darwin) operational C-band Doppler radars to characterize the rainfall, morphological, and
83 dynamical properties of convective systems developing near the coast and propagating offshore, which are
84 particularly poorly forecasted in this region (e.g., Neale and Slingo, 2002; Nguyen et al. 2017a,b), but are thought to
85 contribute about half of the rainfall along tropical coasts (e.g., Bergemann et al. 2015). In this study, we also take
86 advantage of the month-long time series of OceanPOL– Berrimah radar observations to quantify the variability of
87 radar calibration on daily and hourly timescales.

88 The second field experiment (ORCA) was conducted during a transit voyage to relocate *RV Investigator*
89 from Darwin to Perth, Western Australia. This transit voyage was an ideal opportunity to collect collocated radar
90 samples with several operational radars along the coast (Fig. 1). Specific stops of three hours were scheduled in the
91 vicinity of each radar in the event of precipitation within range of OceanPOL and of the ground-based radar. Of the
92 eight possible radars, we have luckily been able to collect such collocated precipitation samples for six of them,
93 except Geraldton and Carnarvon. In this study we will use all these collocated samples to quantify how well the
94 calibration estimate provided for each radar by the GPM technique agree with the calibration estimates obtained
95 using OceanPOL as a second and more accurate source of reference.

96 **2.2 The radars of this study**

97 Table 1 summarizes the relevant information about all radars used in this study. The Australian radar
98 network comprises a large variety of radars from different generations, frequencies (although radars in this study are
99 all C-band radars, other parts of the country are covered by S-band radars), beamwidths (ranging from 1.0° to 1.7°),
100 range resolutions (ranging from 250m to 1000m), and total time to complete each volumetric sampling (from 6 min
101 for more recent radars to 10 minutes for older radars). [Several radars of the network are installed in very remote
102 locations, bringing specific challenges for the regular maintenance and return to service in case of hardware failure.
103 As a result, maintaining an accurate calibration of this network is more difficult than in other countries.](#) At the time
104 of the YMCA and ORCA experiments, all radars operated continuously. The Berrimah (Darwin) and Serpentine
105 (Perth) radars are Tier 1 radars (as they cover capital cities), while all other radars in Table 1 are Tier 2 radars. Tier 1
106 and 2 radars have a calibration accuracy requirement of better than 1 and 2 dB, respectively. The internal calibration
107 accuracy of these operational radars is [ideally](#) checked six-monthly by BoM radar engineers as part of their routine
108 maintenance. [However, periods between visits can be longer for radars in remote locations.](#) The calibration check
109 only includes measurements of gains and losses at different check points of the transmission and reception chains.
110 No end-to-end calibration using external targets is ever performed. Special visits to sites are organized when a radar

111 is down or when complaints are issued by the public about radar data quality. [The extensive recommendations](#)
112 [outlined in Chandrasekar et al. \(2015\) have not been implemented for the Australian radar network yet.](#)

113 The GPM KuPR and OceanPOL radars are the most modern radars. It must be noted that the OceanPOL
114 radar is the only dual-polarization radar. This important feature for several applications is not used in the present
115 study, except for the quality control of the OceanPOL radar data. A critical aspect of operating a radar on a research
116 vessel is the need to compensate for ship motions and velocity in real-time. To do so, the OceanPOL antenna control
117 system ingests the real-time inertial motion unit data from the ship at 10 Hz and steers the radar beam in real-time in
118 the requested azimuth and elevation direction. The accuracy of this stabilization has been found to produce a
119 pointing accuracy better than 0.1°, even in harsh sea conditions. Doppler measurements are automatically corrected
120 in real-time for the Doppler component induced by ship velocity components. Dual-polarization moments are also
121 corrected using the statistical corrections proposed in Thurai et al. (2014). The same calibration procedure as that
122 employed by BoM is used for OceanPOL (internal measurements of gains and losses, no end-to-end calibration).
123 [which does not include the calibration recommendations from Chandrasekar et al. \(2015\).](#)

Deleted: .

124 As discussed previously, the GPM Ku-band radar measurements are considered as the reference for the
125 calibration of all radars in this study. The GPM radar calibration procedure, described in detail in Masaki et al.
126 (2020) inherited from years of calibration work undertaken as part of the previous satellite radar mission, the
127 Tropical Rainfall Measurement Mission (TRMM). This calibration comprises an internal calibration (monitoring
128 closely the gains and losses of each component of the radar) and an external calibration procedure using a ground-
129 based calibrator and sea surface of well-known backscatter. Importantly, the GPM mission also benefits from
130 extensive field experiments undertaken as part of the Ground Validation program, including in-situ ground and
131 aircraft validation of the products of the GPM mission. By comparing different approaches for the GPM Ku-band
132 radar calibration, Masaki et al. (2020) demonstrated that the accuracy of the radar was well within the ± 1 dB
133 requirement. In our study, Version 5 of the GPM 2AKu product has been used for all comparisons in this study
134 (Kidd et al. 2017), which includes the latest calibration from Masaki et al. (2020) and contains attenuation-corrected
135 Ku-band reflectivities. GPM attenuation correction is achieved using a hybrid approach combining the traditional
136 Hitschfeld - Bordan technique (Hitschfeld and Bordan, 1954) and the so-called Surface Reference Technique
137 (Meneghini et al., 2004). To compare GPM Ku-band radar with C-band radars in this study, all GPM Ku-band
138 reflectivities have been converted to their equivalent C-band reflectivities using Eq. 5 in L19.

139 2.3 The S³CAR radar calibration framework

140 Recently, BoM has developed the operational S³CAR (Satellite, Sun, Self-consistent, Clutter calibration
141 Approach for Radars) framework to monitor the calibration of the BoM operational radars in real-time (operational
142 version of L19). This approach is based on a combination of three techniques. The first technique, the Relative
143 Calibration Adjustment (RCA, e.g., L19; Wolff et al. 2015), assumes that the 95th percentile of "ground clutter"
144 radar reflectivities (buildings, topographic structures, trees, etc ...) within 10 km range is constant. This technique
145 tracks changes in daily calibration to better than 0.2 dB (L19) but does not provide an estimate of the absolute
146 calibration. The second technique (W18) statistically compares collocated ground radar and spaceborne Ku-band
147 radar from the NASA TRMM (1997-2014) and GPM (2014-present) missions. The operational implementation of
148 the GPM calibration technique closely follows the description given in W18. Satellite and ground-based radar

150 observations are first matched to a common volume. We require at least a minimum of 10 satellite profiles within
151 the ground radar domain to select and process a satellite overpass. The melting layer is detected by the operational
152 GPM algorithms and excluded from the matched volumes due to uncertainties in frequency conversions for melting
153 hydrometeors. Matched volumes in both liquid and ice phases are retained (like in W18). Non-uniform beam filling
154 effects of the matched volumes are mitigated by only selecting volumes that are 95% filled. A maximum ground-
155 based reflectivity threshold of 36 dBZ is used in the analysis of matched volumes to mitigate the potential impact of
156 attenuation correction errors.

157 From our experience, and as reported in L19, this technique provides an absolute calibration with an
158 accuracy of about 2 dB from each overpass. The S³CAR framework uses the RCA technique to detect stable periods
159 of calibration and averages calibration estimates from all GPM overpasses within each period, improving the
160 absolute calibration accuracy, hopefully to better than 1 dB. Note that these values of 2 dB and 1 dB are qualitative
161 error estimates based on visual inspection of the variability of calibration error estimates from successive satellite
162 overpasses. The third technique used in S³CAR is the solar calibration technique, which is a faithful implementation
163 of the Altube et al. (2015) method, with additional corrections for a possible levelling error of the radars as
164 described in Curtis et al. (2021). The solar calibration technique uses sun power measurements collected at the
165 Learmonth observatory, Western Australia. This technique is mostly used in conjunction with the RCA and GPM
166 outputs to diagnose whether a change in calibration is due to the transmitting chain (RCA and GPM detect a change
167 but not the solar calibration technique) or the receiving chain (all techniques detect a change). This is an important
168 diagnostic to help radar engineers troubleshoot a radar issue and enable rapid return to service.

169 [The BoM does not operate a disdrometer network. As a result, the technique outlined in Frech et al. \(2017\),
170 which compares disdrometer simulations of reflectivity with measured radar reflectivities cannot be added to the
171 S³CAR framework. In the future, with the increasing number of dual-polarization radars in the Australian network,
172 we are planning to investigate the benefits of the so-called self-consistency of polarimetric variables and may add
173 this technique to the framework.](#)

174 Among all operational radars considered in this study, only two of these radars (Berrimah and Geraldton)
175 send the unprocessed reflectivities to Head Office in real-time, allowing for the full S³CAR process to be used to
176 calibrate these radars. The term "unprocessed" here refers to radar data still containing noise and all typical radar
177 signal contaminations, including ground clutter and sun spikes used in our calibration techniques. For the other
178 radars, post-processing is done on-site to reduce the bandwidth required to send the radar data in real-time (these
179 radars are in very remote places). As a result, ground clutter and sun interference have largely been removed for
180 these radars, which implies that only the GPM part of the S³CAR framework can be used. As explained, this reduces
181 the accuracy of the calibration estimate for such radars.

182 **2.4 Statistical comparisons between OceanPOL and the ground radars**

183 Calibration between ground-based radars and OceanPOL proceeds by first gridding observations from each
184 radar to a common 1 km horizontal / 500 m vertical resolution domain, then building a joint frequency histogram of
185 reflectivity values from all common grid points. The expectation from such plots is that they should exhibit a
186 systematic shift, corresponding to a difference in calibration between the two radars, with a large amount of
187 variability in these comparisons owing to all the sources of errors involved in such comparisons (differences in exact
188 time of observations of a grid, imperfect attenuation corrections, gridding artefacts, differences in implicit resolution

189 of radar volumes at different ranges, differences in minimum detectable signal...). The gridding technique used for
190 all radars is the same and follows Dahl et al. (2019). This gridding technique uses a constant radius of influence
191 (3.5 km) and a weighted summation with distance to the centre of the grid for points belonging to the same elevation
192 angle but a linear interpolation in the vertical using data from the elevations below and above each grid. This
193 technique has the advantage of not producing the typical artificial vertical spreading of observations below / above
194 the lowest / highest elevation angles observed when using a radius of influence in all directions. Depending on how
195 old the ground radars are, different minimum reflectivity thresholds are used in the comparisons to mitigate potential
196 artefacts in calibration difference estimates due to the degraded sensitivity and reflectivity resolution of the older
197 radars for low to intermediate reflectivities. In general, a relatively high threshold of 20-25 dBZ was required, which
198 also had the advantage of reducing the potential impact of different non-uniform grid filling at the edges of the
199 convective systems due to different radar detection capabilities.

200 OceanPOL data have been corrected for attenuation using the Gu et al. (2011) C-band dual-polarization
201 technique available in the Py-ART toolkit (Helmus and Collis, 2016). The operational radars have been corrected for
202 attenuation using C-band reflectivity – attenuation relationships derived from the OceanRAIN dataset (Protat et al.
203 2019). It must be noted that additional comparisons done without attenuation corrections of the ground radars did
204 not yield large differences (less than 0.5 dB in all sensitivity tests conducted). This is presumably due to the fact that
205 there are many more points below 30-35 dBZ than above in those comparisons, resulting in a relatively minor
206 impact of attenuation on these statistical comparisons. Also, the ship and ground radars were generally not far away
207 from each other (typically 20-40 km), so the viewing geometry of the storms was quite similar from both radars in
208 most cases, resulting in similar levels of attenuation along the two different paths through the storms.

209 The scanning sequence employed for OceanPOL uses the exact same 14 elevation angles used throughout
210 the operational radar network. The start of each OceanPOL scanning sequence is synchronized with that of the
211 operational radars running a 6-minute sequence (starts on the hour then every 6 minutes), which implies that
212 temporal differences in volumes sampled by OceanPOL and the radars running the 6-minute sequence are minimal.
213 The impact of temporal evolution on the comparisons between OceanPOL and the radars running a 10-minute
214 sequence will naturally be larger. To minimize this impact in our comparisons, we have discarded files for which the
215 start time differs from the OceanPOL start time by more than 2 min.

216 Finally, to mitigate the potential impact of wet radome attenuation at C-band on the comparisons, we have
217 screened out observations where precipitation was present within 5 km of either of the radars from the comparisons.
218 More precisely, for each volumetric scan we estimate the precipitation fraction within 5 km, and if more than 20 %
219 of this area is covered with precipitation, we conservatively discard this scan. However, it must be noted that results
220 obtained when changing that threshold were very similar, with maximum statistical differences in estimated
221 calibration difference less than 0.3 dB (not shown). From a visual inspection of radar scans, we inferred that this was
222 due to rainfall generally not observed over and around the radars when such comparisons were made.

223
224
225

226 **3 Results**

227 In this section, we present the main results of this three-way calibration comparison exercise. Comparisons
228 between OceanPOL and the ground-based radars, all calibrated using GPM, are used to quantify the accuracy of the
229 GPM VMM technique. The day-to-day variability of ground – ship radar comparisons over a month is also used to
230 quantify the accuracy of daily calibration monitoring using overlapping ground-based radars and its potential for
231 operational use. Lastly, we explore the potential for tracking calibration differences at the hourly time scale rather
232 than the daily time scale using overlapping ground-based radars.

233 **3.1 The accuracy of the GPM VMM technique**

234 As illustrated in Fig. 1, the first part of the calibration consistency check is to calibrate OceanPOL and the
235 ground radars using the same single independent source, the GPM spaceborne radar. All calibration results are
236 summarized in Fig. 2. We are fortunate enough that over two months including the YMCA and ORCA observational
237 periods, the rainfall activity allowed us to collect a reasonable number of GPM overpasses over each radar (except
238 for Learmonth, radar 29, Fig. 2). As a result, for radar 29, we will use an older calibration estimate (-2.6 dB),
239 derived from a GPM overpass with many matched volumes in July 2019 and will assume that its calibration has not
240 changed. As discussed previously, the RCA technique can be used to accurately track changes in calibration.
241 Unfortunately, among all radars included in Fig. 2, the RCA can only be applied to radar 63. Additional checks of
242 the outputs of the RCA technique for radar 63 (not shown) indicated that the calibration of radar 63 had not changed
243 over that period, which means that we can simply average all the estimates of calibration error from individual
244 overpasses to come up with a more accurate estimate for this radar 63. ~~Although the RCA technique cannot be used~~
245 ~~for the other radars, some insights into the calibration stability can be gained from individual calibration estimates~~
246 from individual GPM overpasses in each panel of Fig. 2. Considering the expected typical error of 2 dB for
247 individual GPM overpasses as a guideline, it seems reasonable to assume that the calibration of the OceanPOL,
248 Waruwi (77), Dampier (15), Broome (17), and Serpentine (70) radars has not changed over the observational period
249 either, with fluctuations around the mean calibration error estimate less than ~1.5 dB. Results using the solar
250 calibration technique for OceanPOL also indicate that the OceanPOL receiver calibration has remained constant, to
251 within 1 dB, over the study period (sun power of about -93 dBm). The Port Hedland (16) radar is more problematic,
252 as the time series shows calibration error estimates ranging from -8 dB to -2.5 dB over that period. However, the
253 three overpass points closest to the date when collocated observations with OceanPOL were collected (26 December
254 2019) seem to agree reasonably well (around the mean value of -5 dB), so we will use this value of -5 dB in the
255 following but will keep in mind the lower confidence in this calibration figure.

256 The final step of this calibration consistency check study consists in using the OceanPOL radar (previously
257 calibrated using GPM, Fig. 2) as a second moving reference to compare with the ground-based radars. As explained
258 earlier, satellite – ground comparisons are characterized by multiple sources of errors, including differences in
259 sampled volumes (although great care is taken to match sampling volumes as accurately as possible, e.g., Schwaller
260 and Morris 2011, W18, L19), non-uniform beam filling effects, temporal mismatch between observations,
261 differences in minimum detectable signal, and radar frequency differences requiring conversion (most problematic
262 in the melting layer and ice phase of convective storms where this correction is more uncertain, see W18). In
263 comparison, ship radar – ground radar comparisons, especially when radars are, as in this study, reasonably close to

Deleted:

Deleted: the

266 each other to minimize differences in sampling volumes, are less prone to all these errors. The radar frequency is the
267 same. The sampling volume and temporal mismatches are also expected to be less problematic (but not entirely
268 negligible, especially for the radars running a 10-min sequence, see discussion in section 2.4). These more accurate
269 ship – ground radar comparisons should therefore be considered as an indirect evaluation of the GPM validation
270 technique and if successful, a demonstration of the value of using such GPM data as a single source of reference for
271 the calibration of a whole national network as is done in Australia with S³CAR.

272 Figure 3 shows an example of the 2D frequency histograms of reflectivity that are used to estimate
273 calibration differences between OceanPOL and any of the radars. This particular figure is for the Berrimah radar
274 (63) for one day (21 November 2019) of the YMCA experiment. Such frequency distribution plots can be
275 normalized in two different ways. If the number of points in each reflectivity pixel is divided by the total number of
276 points (as in Fig. 3a), it highlights where most of the comparison points are in the reflectivity – reflectivity space,
277 and therefore what contributes most to the mean calibration difference estimate. When the number of points in each
278 pixel is divided by the total number of points in each reflectivity bin on the x-axis (Fig. 3b), the joint distribution
279 provides a better visual sanity check of the systematic shift of the joint distribution produced by the calibration
280 difference over the whole reflectivity range and allows detection of other potential artefacts. In the example of Fig.
281 3a, which is typical of all comparisons made in this study, it is clear that reflectivities less than 35 dBZ contributed
282 most to the estimation of the mean calibration difference of 0.9 dB between the two radars. On another hand, Fig.
283 3b shows more clearly that there is indeed a consistent shift in reflectivity values across the whole reflectivity range,
284 as expected from a (systematic) calibration difference. An important feature of Fig. 3 is the observed large
285 variability around the mean calibration difference. The standard deviation of calibration difference for all
286 comparisons in this study was typically between 4 and 6 dB. It must be noted that this large standard deviation is an
287 estimation of the errors on calibration difference of each individual pixel, not that of the daily estimate. The higher
288 number of days spent collecting collocated observations off the Berrimah (63) and Waruwi (77) radars also offers
289 an opportunity to estimate daily calibration differences and take a closer look at the day-to-day variability of
290 calibration differences.

291 When including all days of observations for radars 63 and 77 (25 days for radar 63 and 4 days for radar 77
292 with precipitation), the mean calibration difference between OceanPOL and radars 63 and 77 are 0.4 dB and -0.3
293 dB, respectively (see Fig. 4 for radar 63, Fig. 5a for radar 77, see also Table 2 for a summary of all calibration
294 differences found in this study). The other relatively recent, better-quality operational radar included in this study is
295 radar 70 (Perth). For this radar, only short duration drizzle and scattered showers were observed when *RV*
296 *Investigator* approached its destination (Fremantle port), resulting in less points for the calibration difference
297 estimate. Despite the short duration dataset for radar 70, the 2D joint histogram of reflectivities show a consistent
298 difference across the whole reflectivity range, with a mean calibration difference of -0.4 dB (Fig. 5f). These three
299 estimates are well below the required accuracy of 1 dB for operational applications, which indicates that for these
300 four good-quality radars (OceanPOL and radars 63, 77, and 70), the GPM comparisons provided a consistent
301 calibration to within ± 0.5 dB. However, those are the comparisons where errors were expected to be smallest, given
302 the large number of days included in the comparisons for radars 63, and the excellent synchronization of the 6-min
303 scanning sequences with OceanPOL for these three radars.

304 Let us now turn our attention to the quantitative comparisons between OceanPOL and the older operational
305 radars (15, 16, 17, 29) running with a 10-minute scanning sequence and/ or a degraded range resolution (as reported
306 in Table 1), and only a few opportunistic hours of collocated samples with precipitation (see list of time spans in
307 Table 2). Visual inspection of gridded radar data revealed the presence of strong anomalous propagation (AP) signal
308 in the lower levels (up to about 2km height ASL) for radars 15, 16, and 29, which has not been filtered correctly by
309 the operational radar post-processing suite. This problem is well known to the BoM forecasters. As a result, for these
310 radars, two sets of results are presented in Table 2. Calibration differences obtained from all data are labelled "AP"
311 and those obtained when screening out all common grids below 2km height are labelled "noAP". Figure 5 shows the
312 2D joint histograms of reflectivity when the anomalous propagation is screened out. The largest impact of
313 anomalous propagation is found for radar 16, with a difference of 0.9 dB between estimates with and without AP
314 screening. For the two other radars 15 and 29, the impact is modest (0.3 to 0.5 dB). This is due to the higher
315 proportion of samples located below 2 km height for the radar 16 case (not shown) than for the two other cases.
316 Overall, this result is shown to illustrate that particular attention needs to be paid in regions prone to anomalous
317 propagation effects. From Table 2 and Fig.5, the calibration differences with OceanPOL for these older radars are
318 +0.3 dB (radar 15), +0.1 dB (radar 16), +0.4 dB (Broome, radar 17), and +0.1 dB (radar 29). In summary, all seven
319 radars considered in these comparisons are characterized by calibration differences with OceanPOL within +0.5 dB,
320 despite the large variability in radar quality and number of samples included in the calibration difference estimates
321 (reported in Fig. 5). As a result, we can safely conclude that these comparisons validate the concept of using the
322 GPM VMM calibration technique as a single source of reference to accurately calibrate and monitor calibration of
323 national radar networks.

324 **3.2 The accuracy of daily calibration monitoring from overlapping ground-based radars**

325 As introduced earlier, the day-to-day variability of calibration differences between ship and ground-based
326 radars can be analysed using the month of collocated samples between OceanPOL and the Berrimah radar collected
327 during YMCA (coloured points in Fig. 4). From Fig. 4, some simple statistics can be derived and discussed. The
328 minimum and maximum calibration differences over the month-long time series are -0.2 and +1.1 dB, which
329 corresponds to minimum and maximum differences of -0.6 and +0.7 dB around the mean value of 0.4 dB. The
330 colour of the points is the number of samples that were available to estimate the daily calibration difference. The
331 coloured error bars are estimates of the hourly standard deviation of calibration difference for each day. From a
332 close inspection of the location of points with respect to the mean value for the period, there does not seem to be any
333 obvious relationship between the number of points and how close the estimates are to the mean value of 0.4 dB. This
334 result shows that the number of samples is not the main source of differences between daily estimates.

335 The standard deviation of daily calibration difference between Berrimah and OceanPOL over this month of
336 data is 0.33 dB (Fig. 4). Since this standard deviation value includes any potential natural variability of the daily
337 calibration difference and the variability due to uncertainties in these daily ship – ground radar comparisons such as
338 spatial resolution differences and temporal mismatches, this value of 0.33 dB can be considered as an upper bound
339 for the uncertainty in daily calibration difference estimates. To check whether the natural variability of daily radar
340 calibration was minimal over that month of Darwin observations, we have added in Fig. 4 the time series of daily
341 mean RCA values (black points) used as part of our operational S³CAR calibration monitoring technique as another
342 calibration variability metrics. It has been shown that this RCA technique could track changes in daily calibration to

343 better than about 0.2 dB (L19). To better compare variabilities obtained from calibration differences and the RCA,
344 we have subtracted the mean RCA (54.11 dBZ) value to each daily RCA value and added the mean calibration
345 difference over the whole period (0.4 dB), so that the daily RCA time series is centred on the mean calibration
346 difference (blue line). Over this whole period, the standard deviation of the RCA value is 0.12 dB, which confirms
347 the L19 results. This standard deviation is smaller than that of the OceanPOL–Berrimah comparisons (0.33 dB). If
348 we assume that the standard deviation of the RCA value is an upper bound for the natural variability of the daily
349 calibration figure, this result shows that most of the variability in calibration difference between the OceanPOL and
350 Berrimah radars (0.33 dB) is in fact a measure of the inherent uncertainties of gridded radar comparisons. This
351 important result highlights that such quantitative comparisons of overlapping gridded radar observations can be
352 successfully used to monitor the consistency of daily calibration of operational radars with overlapping coverage to
353 better than the 1 dB requirement.

354 **3.3 The accuracy of hourly calibration monitoring from overlapping ground-based radars**

355 The last thing we explore with this Darwin dataset is the potential for tracking calibration differences at the
356 hourly time scale rather than the daily time scale. To do so, for each day of observations, we have estimated the
357 calibration difference from 1-hour chunks of collocated data, then estimated the standard deviation of the hourly
358 estimates for each day. An example of such daily analysis is shown in Fig. 6 for a day (08/12/2019) where 15
359 successive hours of collocated samples were available. Although this example includes more hours of comparisons
360 than most other days, it is very typical in terms of the hour-to-hour variability we observe each day, making it a
361 good candidate for illustrative purposes. We have not elected to screen out hours with fewer points, which, as can be
362 seen from hours 14 and 15, would have resulted in a lower hourly standard deviation for that case. This should
363 probably be done in an operational implementation. In this respect, the standard deviation of hourly calibration
364 difference presented in Fig. 4 can be considered as an upper bound for the hourly standard deviation. The hourly
365 standard deviation is shown in Fig. 6 as a red error bar on top of the daily average point, and as a coloured error bar
366 over each daily average in Fig. 4. Over the 1-month study period, the average hourly standard deviation derived
367 from all hourly estimates is 0.8 dB, which is within the 1 dB requirement, but the two extreme values are 0.5 and 1.5
368 dB (Fig. 4), indicating that occasionally the hourly estimates of calibration difference would not fully meet this
369 requirement. From Fig. 4, it also appears that there is no inverse relationship between the number of samples and the
370 hourly standard deviation, which could have perhaps been expected. For instance, the two points with highest hourly
371 standard deviation (02 and 06 December 2019) are at both ends of the number of samples spectrum, and the three
372 points with the lowest hourly standard deviations are in the lower half of the number of samples spectrum. Fig. 4 also
373 shows that when using the hourly standard deviation as an error bar, the mean value over that period (0.4 dB) is
374 always included within one standard deviation of the daily estimate. These results would obviously need to be
375 confirmed with more observations in the future but do highlight the potential for hourly tracking of calibration
376 differences, enabling very early detection of issues with operational radars.

377

378

379

380 **4 Conclusions**

381 In this study, we have used collocated observations between spaceborne, ship-based, and ground-based
382 radars collected during the YMCA (off Darwin) and ORCA (transit voyage between Darwin and Perth) experiments
383 to gain further insights into the suitability and accuracy of using spaceborne radar observations from the GPM
384 satellite mission to calibrate national operational radar networks, and to assess the potential of using data from
385 overlapping ground-based radars to track calibration changes operationally at the daily and hourly time scales.

386 A major advantage of the GPM VMM technique is that all radars of the network are calibrated against a
387 single source of reference. The GPM VMM literature (Schwaller and Morris, 2011; W18; L19) suggests that errors
388 are of about 2 dB from individual GPM overpasses to better than 1 dB when stable periods of calibration can be
389 estimated using the RCA technique and individual GPM estimates can be averaged. However, these errors have
390 never been fully quantified. Using collocated weather radar observations between the OceanPOL radar on *RV*
391 *Investigator* and 7 operational radars off the northern and western coasts of Australia (all calibrated using GPM), we
392 found that for all seven operational radars, the calibration difference with OceanPOL was within ± 0.5 dB, well
393 within the 1 dB requirement for quantitative radar applications (-0.3, +0.4, +0.4, +0.1, +0.3, +0.1, and -0.4 dB). This
394 important result validates the concept of using the GPM spaceborne radar observations to calibrate national weather
395 radar networks.

396 From the longer YMCA dataset collected when *RV Investigator* was stationed off the coast of Darwin for
397 about a month, the day-to-day variability of calibration differences between the OceanPOL and Darwin (Berrimah)
398 radars was estimated and compared with the daily calibration variability estimated using the RCA technique. From
399 these comparisons, we found that the natural variability of daily radar calibration was small over our month of
400 observations (~ 0.1 dB daily standard deviation). These comparisons also demonstrated that the intercomparison of
401 gridded radar observations had the potential to estimate calibration differences between radars with overlapping
402 coverage to within about 0.3 dB at daily time scale and about 1 dB at hourly time scale. Such technique will be
403 added to our operational S³CAR calibration monitoring framework as an additional calibration monitoring reference
404 between GPM overpasses when the RCA technique cannot be applied.

405 **Acknowledgments**

406 The Authors wish to thank the CSIRO Marine National Facility (MNF) for its support in the form of *RV Investigator*
407 sea time allocation on Research Voyages IN2019_V06 (YMCA) and IN2019_T03 (ORCA), support personnel,
408 scientific equipment, and data management. Tom Kane and Mark Curtis from BoM are also warmly thanked for
409 always patiently answering our relentless questions about the Australian weather radar network intricacies.

410 **Code availability**

411 Codes developed for this study are protected intellectual property of the Bureau of Meteorology and are not publicly
412 available.

413 **Data availability**

416 All OceanPOL and Level 1b data from the operational radar network used in this study are available at
417 <http://www.openradar.io>. The NASA GPM radar data were obtained using the STORM online data access interface
418 to NASA's precipitation processing system archive (<https://storm.pps.eosdis.nasa.gov>).

419

420 **Sample availability**

421 No samples were used in this study.

422

423 **Author contribution**

424 AP, JS, VL, JB, and WP collected the datasets used in this study. VL produced the GPM comparisons using the
425 operational S3CAR technique. JS produced post-processed volumetric and gridded data for all ground-based radars.
426 VL produced the gridded OceanPOL data. JB developed the gridding technique used in this study. AP designed and
427 coordinated the YMCA and ORCA field experiments, analyzed the results, and wrote the manuscript. VL, JS, JB,
428 and WP provided edits of the manuscript.

429

430 **Competing interests:**

431 The authors declare that they have no conflict of interest.

432

433

434

435 **References**

436 Altube, P., J. Bech, O. Argemi, and T. Rigo: Quality control of antenna alignment and receiver calibration using the
437 sun: Adaptation to midrange weather radar observations at low elevation angles. *J. Atmos. and Ocean. Technol.*,
438 32, 927-942, 2015.

439 Bergemann, M. M., C. Jakob, and T. P. Lane: Global detection and analysis of coastline-associated rainfall using an
440 objective pattern recognition technique. *Journal of Climate*. 28, 18, p. 7225-7236, 2015.

441 [Chandrasekar, V., L. Baldini and N. Bharadwaj and P. L. Smith, 2015: Calibration procedures for global
442 precipitation-measurement ground-validation radars. *URSI Radio Science Bulletin*, 355, 45-73.](#)

443 Curtis, M., G. Dance, V. Louf, and A. Protat: Diagnosis of Tilted Weather Radars Using Solar Interference. *J.*
444 *Atmos. Oceanic Tech.*, 38, 1613-1620, 2021.

445 Dahl, N. A., A. Shapiro, C. K. Potvin, A. Theisen, J. G. Gebauer, A. D. Schenkman, and M. Xue: High-Resolution,
446 Rapid-Scan Dual-Doppler Retrievals of Vertical Velocity in a Simulated Supercell. *J. Atmos. and Ocean.*
447 *Technol.*, 36, 1477-1500, 2019.

448 [Frech, M., M. Hagen, and T. Mammen: Monitoring the Absolute Calibration of a Polarimetric Weather Radar. *J.*
449 *Atmos. and Ocean. Technol.*, 34, 3, 599-615, 2017.](#)

450 Gu, J.-Y., A. Ryzhkov, P. Zhang, P. Neille, M. Knight, B. Wolf, and D.-I. Lee: Polarimetric Attenuation
451 Correction in Heavy Rain at C Band. *Journal of Applied Meteorology and Climatology*, 50(1), 39-58, 2011.

452 Helmus, J. J., and S. M. Collis.: The Python ARM Radar Toolkit (Py-ART), a Library for Working with Weather
453 Radar Data in the Python Programming Language. *Journal of Open Research Software*, 4(1), e25, 2016.

Deleted:

455 Hitschfeld, W., and J. Bordan: Errors inherent in the radar measurement of rainfall at attenuating wavelengths.
456 J. Meteor., 11, 58–67, 1954.

457 Hou, A. Y., and Coauthors: The Global Precipitation Measurement mission. Bull. Amer. Meteor. Soc., 95, 701–722,
458 2014.

459 Kidd, C., J. Tan, P.-E. Kirstetter, and W. A. Petersen: Validation of the Version 05 Level 2 precipitation products
460 from the GPM core observatory and constellation satellite sensors. QJR Meteorol Soc., 144, 313–328.

461 Kollias, P., B. Puigdomènech Treserras, and A. Protat: Calibration of the 2007–2017 record of ARM Cloud Radar
462 Observations using CloudSat, *Atmos. Meas. Tech.*, 12, 4949–4964, 2019.

463 Louf, V., A. Protat, C. Jakob, R. A. Warren, S. Rauniar, W. A. Petersen, D. B. Wolff, and S. Collis: An integrated
464 approach to weather radar calibration and monitoring using ground clutter and satellite comparisons. J. Atmos.
465 Oceanic Tech., 36, 17–39, 2019. (L19)

466 Masaki, T., T. Iguchi, K. Kanemura, K. Furukawa, N. Yoshida, T. Kubota, and R. Oki: Calibration of the Dual-
467 Frequency Precipitation Radar Onboard the Global Precipitation Measurement Core Observatory. IEEE
468 TRANSACTIONS ON GEOSCIENCE AND REMOTE SENSING, 2020.

469 Meneghini, R., J. Jones, T. Iguchi, K. Okamoto, and J. Kwiatkowski: A hybrid surface reference technique and its
470 application to the TRMM precipitation radar. J. Atmos. Oceanic Technol., 21, 1645–1658, 2004.

471 Neale, R., and J. Slingo: The maritime continent and its role in the global climate: A GCM study, J. Clim., 16, 834–
472 848, 2002.

473 Nguyen, H., C. Franklin, and A. Protat: Understanding model errors over the Maritime Continent using CloudSat
474 and CALIPSO simulators. Quart. J. Roy. Meteor. Soc., 2017.

475 Nguyen, H., A. Protat, L. Rikus, H. Zhu and M. Whimpey: Sensitivity of the ACCESS forecast model statistical
476 rainfall properties to resolution. Quart. J. Roy. Meteor. Soc., 2017.

477 Protat, A. and I. McRobert: Three-dimensional wind profiles using a stabilized shipborne cloud radar in wind
478 profiler mode. Atmos. Meas. Tech., 13, 3609–3620, 2020.

479 Protat, A., C. Klepp, V. Louf, W. Petersen, S. P. Alexander, A. Barros, and G. G. Mace: The latitudinal variability
480 of oceanic rainfall properties and its implication for satellite retrievals. Part 2: The Relationships between Radar
481 Observables and Drop Size Distribution Parameters. J. Geophys. Res. Atmos., 124, 13312–13324, 2019.

482 Schwaller, M. R., and K. R. Morris: A ground validation network for the Global Precipitation Measurement mission.
483 J. Atmos. Oceanic Technol., 28, 301–319, 2011.

484 Simpson, J., C. Kummerow, W.-K. Tao, and R. F. Adler: On the Tropical Rainfall Measuring Mission (TRMM).
485 Meteor. Atmos. Phys., 60, 19–36, 1996.

486 Thurai, M., P. T. May, and A. Protat: Shipborne polarimetric weather radar: Impact of ship movement on
487 polarimetric variables. J. Atmos. Oceanic Tech., 31, 1557–1563, 2014.

488 Warren, R. A., A. Protat, V. Louf, S. T. Siems, M. J. Manton, H. A. Ramsay, and T. Kane: Calibrating ground-based
489 radars against TRMM and GPM. J. Atmos. Oceanic Tech., 35, 323–346, 2018. (W18)

490 Wolff, D. B., D. A. Marks, and W. A. Petersen: General application of the relative calibration adjustment (RCA)
491 technique for monitoring and correcting radar reflectivity calibration. J. Atmos. Oceanic Technol., 32, 496–506,
492 2015.

493

494

Formatted: Font: Italic

Radar ID or Platform	Name	Make	(lat, lon)	Band	$\omega(^{\circ})$	$\Delta r(m) /$ $\Delta t(min)$
GPM	KuPR	N/A	Variable	Ku	0.7	125 / NA
RV Investigator	OceanPOL	DWSR-2501C-SDP	Variable	C	1.3	125 / 6
15	Dampier	WSR81C	(-20.654; 116.683)	C	1.7	1000 / 10
16	Port Hedland	TVDR2500-8	(-20.372; 118.632)	C	1.7	500 / 10
17	Broome	DWSR2502C-8	(-17.948; 122.235)	C	1.7	500 / 10
29	Learmonth	TVDR2500-8 (Digital upgrade)	(-22.103; 113.999)	C	1.7	250 / 10
63	Berrimah (Darwin)	DWSR2502C-14	(-12.456; 130.927)	C	1.0	250 / 6
70	Serpentine (Perth)	TVDR2500-14	(-32.392; 115.867)	C	1.0	500 / 6
77	Waruwi	DWSR2502C-14	(-11.648; 133.380)	C	1.0	250 / 6

496 Table 1: Main characteristics of the radars used in this study: radar ID in the operational radar network or platform,
497 name, make, coordinates, frequency band, beamwidth $\omega(^{\circ})$, range bin size $\Delta r(m)$, and total time to complete the
498 volumetric sampling $\Delta t(min)$. OceanPOL and all ground-based radars have been manufactured by the Enterprise
499 Electronics Corporation (EEC).

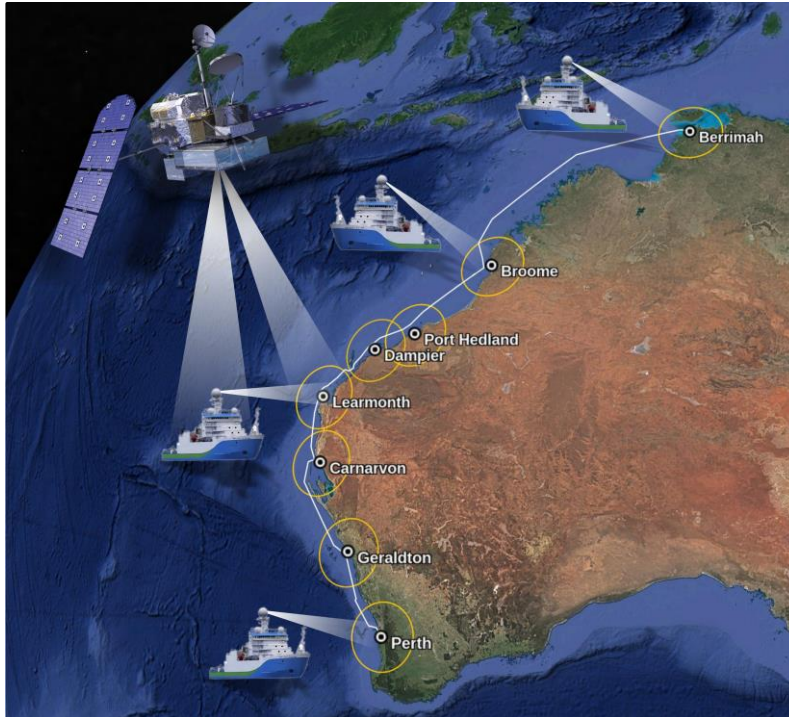
500

Date	Time Span (UTC)	Radar	Calibration Error (Radar – OceanPOL)
20191115	04:00 – 07:00	77	-0.2
20191117	04:00 – 08:00	77	+0.5
20191127	06:00 – 11:00	77	-0.2
20191128	03:00 – 07:00	77	-0.6
All dates above	All time spans above	77	-0.3
All dates in Fig. 4	Miscellaneous	63	+0.4
20191225	12:00 – 21:00	17	+0.4
20191226	18:00 – 24:00	16	-0.8 (AP) / +0.1 (noAP)
20191227	08:00 – 11:00	15	-0.2 (AP) / +0.3 (noAP)
20191228	08:00 – 11:00	29	-0.2 (AP) / +0.1 (noAP)
20200102	03:00 – 05:00	70	-0.4

501 Table 2: Ground radar – OceanPOL calibration difference estimates for all comparisons of this study. A mean
502 calibration difference for radars 63 and 77 that includes all dates and time spans is also provided. For radars 15,
503 and 29, two estimates are provided, with no test on minimum height (AP) or with a minimum height of 2 km for the
504 comparisons (noAP), in an attempt to remove residual anomalous propagation artefacts observed for these radars.

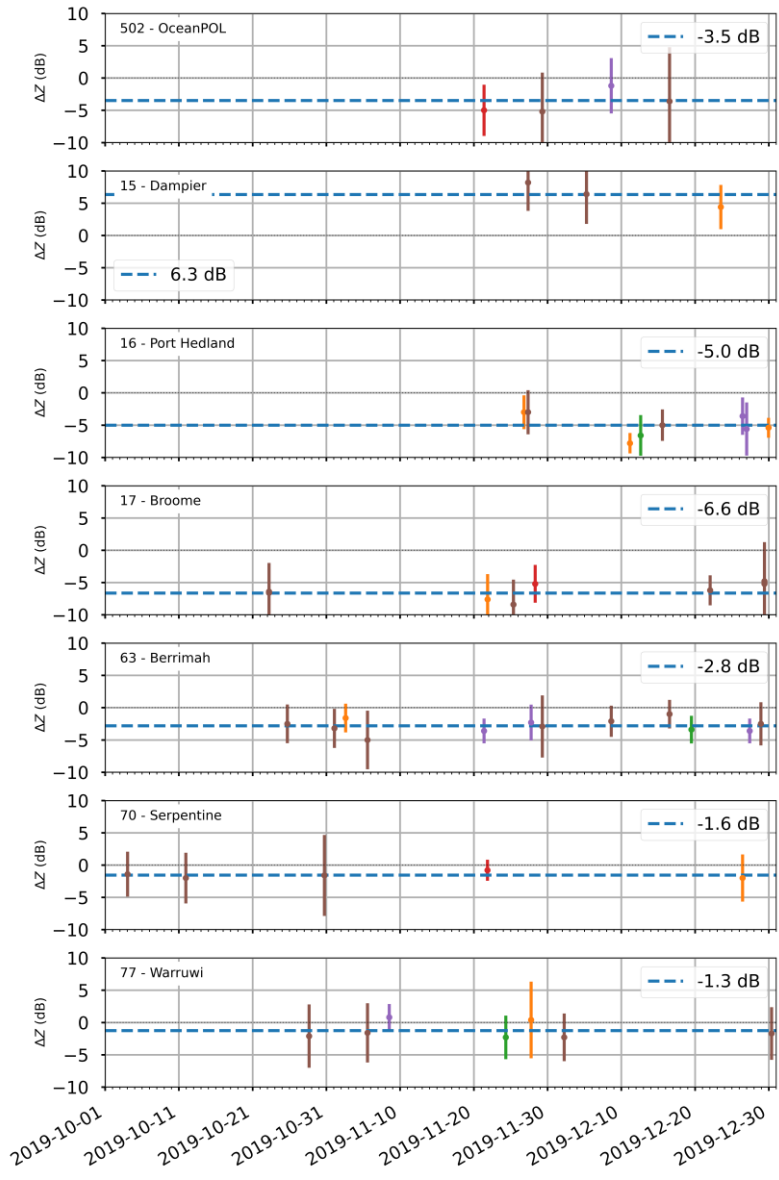
505

506

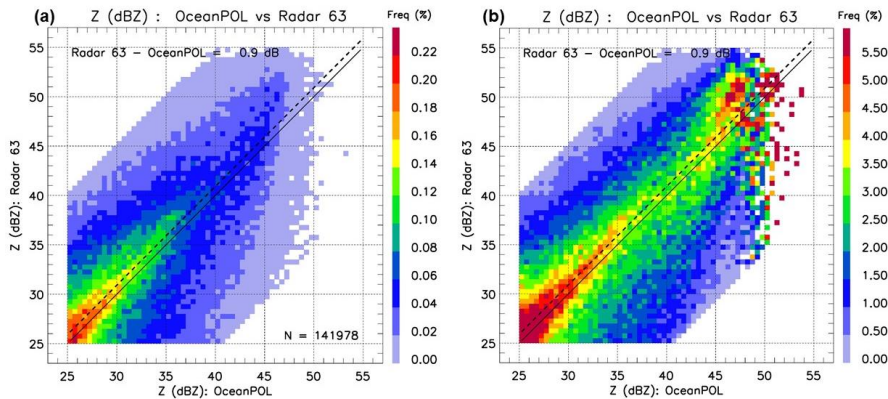


508

509 Figure 1: The concept of this study. Ship-based OceanPOL radar and ground-based radars are calibrated independently
510 using the GPM Ku-band spaceborne radar, then all ground radars are compared with OceanPOL during the ORCA
511 voyage as RV Investigator sails south. The 150 km radius of each radar is shown by a yellow circle and the ship track is
512 shown using a white line. © 2021 Google Earth; Map Data: SIO, NOAA, U.S. Navy, NGA, GEBCO; Map Image:
513 Landsat/Copernicus.



514
 515 **Figure 2: Individual calibration error estimates from the GPM comparisons, for all radars used in this study. The**
 516 **standard deviation of the PDF of reflectivity difference is also shown for each estimate as an error bar. The mean value**
 517 **over the whole period is displayed as a dashed line for each radar, and the value is reported on the upper-right of each**
 518 **panel. Note that a negative value mean that the radar is under-calibrated (radar – GPM). The colour of each overpass**
 519 **point is the number of matched volumes: less than 20 (blue), 20 to 60 (orange), 60 to 100 (green), 100 to 150 (red), 150 to**
 520 **200 (purple) or more than 250 (brown).**



521

522

523

524

525

526

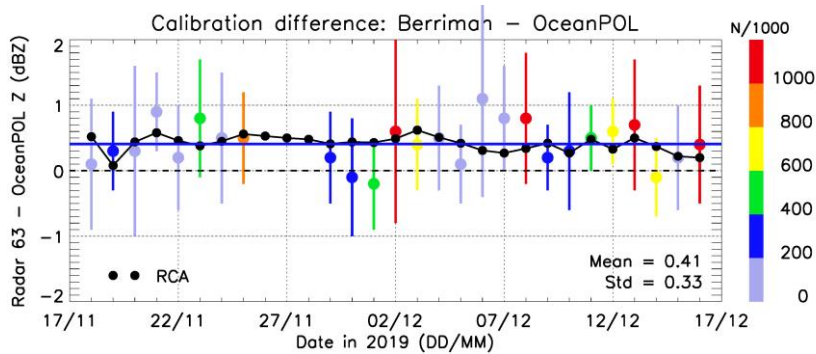
527

528

529

530

Figure 3: Illustration of 2D joint frequency histograms of reflectivity used to compare quantitatively the OceanPOL radar (x-axis) and any of the ground-based radar (y-axis), here for the Berrimah radar (63) for one day (21 November 2019) of the YMCA experiment. For each plot, the 1:1 line is drawn as a solid line, and the calibration difference estimate is written and shown as a dashed line. The colours show the frequency of points falling in each reflectivity pixel 0.5 dB in resolution of the 2D joint histograms, either expressed as the % of the total number of points (panel a) or as a % of the sum of points for each value of OceanPOL reflectivity (i.e., sum of all points along the y-axis at each constant value of the x-axis). The number of samples N for this case is 141978 (see panel a).



531

532

533

534

535

536

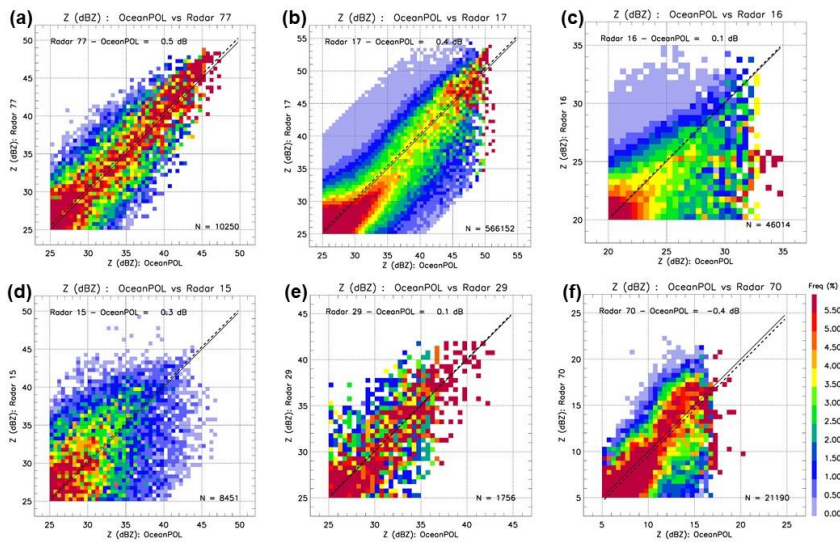
537

538

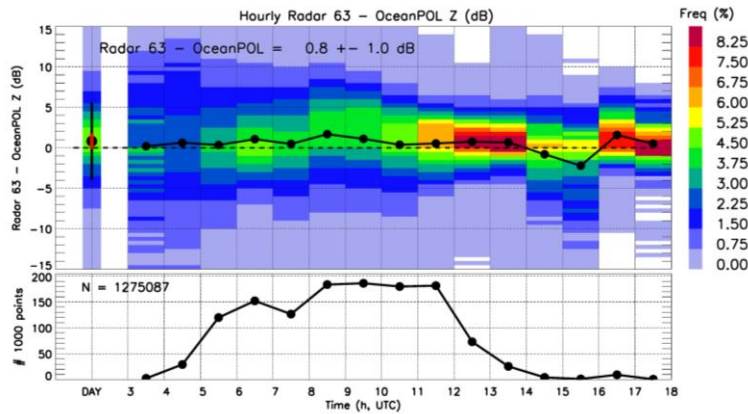
539

540

Figure 4: Time series of calibration differences between OceanPOL and radar 63 (Berrimah) during the YMCA experiment. Each coloured point is a daily estimate of calibration difference. The colour of the point is the number of points for each comparison, and the coloured error bar is the standard deviation of hourly calibration difference estimates for that day (see text and Fig. 6 for more details). The solid blue line is the mean value obtained from all these daily estimates (0.4 dB). The overall mean and standard deviation of the daily calibration difference over the period of observations are also written on the lower-right side of the figure. The black dashed line is the zero line. The black points are the daily outputs of the RCA values, with the mean RCA value over the period subtracted and the mean value of calibration difference added, so that the time series is centred on the mean calibration difference value.



541
 542 **Figure 5:** 2D joint histograms of reflectivity as in Figure 3b but for radars (a) 77, (b) 17, (c) 16, (d) 15, (e) 29, and (f) 70.
 543 Values of calibration differences are also reported in Table 2. The number of samples N is also given in each panel.
 544



545
 546 **Figure 6:** Hourly analysis of calibration differences between Berrimah (radar 63) and OceanPOL for a selected day
 547 (08/12/2019). The upper panel shows each hourly calibration estimate as a black dot, as well as the full frequency
 548 distribution of differences within each hour (colours). The first column of the upper-panel shows the daily summary,
 549 including the mean value (black dot, value is also written), the frequency distribution of calibration differences (colours),
 550 the standard deviation of the difference using the N collocated samples (black error bar), and the standard deviation of
 551 the hourly estimates of calibration differences for that day (red error bar, value is also written). Lower panel shows the
 552 number of samples in each hour (note y axis is the number of points divided by 1000) and the total number of samples N
 553 is also provided.